Observation of Interfacial Instability of an Ultrathin Water Film

Yoko Tomo,[1,*] Sarthak Nag,[1,2] and Hiroshi Takamatsu[1]
[1]Department of Mechanical Engineering, Kyushu University, Fukuoka 819-0395, Japan
[2]International Institute for Carbon-Neutral Energy Research (WPI-I2CNER), Kyushu University, Fukuoka 819-0395, Japan

(Received 26 January 2021; revised 6 February 2022; accepted 3 March 2022; published 6 April 2022)

We observed the instability of a few-nanometer-thick water film encapsulated inside a graphene nanoscroll using transmission electron microscopy. The film, that was left after recession of a meniscus, formed ripples along the length of the nanoscroll with a distance only 20%–44% of that predicted by the classical Plateau-Rayleigh instability theory. The results were explained by a theoretical analysis that incorporates the effect of the van der Waals interactions between the water film and the graphene layers. We derived important insights into the behavior of liquid under nanoscale confinement and in nanofluidic systems.

DOI: 10.1103/PhysRevLett.128.144502

Nanofluidic [1] systems have drawn great interest over the past fifteen years because of potential applications in ion pumps [2], DNA analyses [3], water desalination [4], and osmotic energy harvesting [5]. Molecular dynamics simulations and experiments have uncovered unique behaviors of ultrafast water flows in carbon nanochannels [6,7] that exceed Hagen-Poiseuille flow. Freezing in carbon nanotubes [8,9] has also been reported, which was unexpected from nucleation theory based on interfacial tension. These exotic phenomena stem from strong atomic and molecular interactions. However, there is little understanding as to how these interactions affect fluidic behaviors. Specifically, dynamics over the range of several to dozens of nanometers are poorly understood because this length scale is too large for molecular dynamics simulations and too small for optical microscope observations. Recent developments in liquid-phase electron microscopy [10] have provided a method for *in situ* observations of water molecules under confinement [11], phase transitions [12], interfacial dynamics [13], and morphologies [14,15] in one-dimensional nanoscale channels. However, there remains a need to establish a better understanding of behaviors observed with a transmission electron microscope (TEM). The interpretation of broader TEM datasets will be important for characterizing behaviors at these length scales and for understanding phenomena that do not follow existing laws or theories.

Here, we report *in situ* observations of ultrathin water film instabilities in a nanoscale channel inside a graphene nanoscroll (GNS) [13,16,17], which is a relatively new type of one-dimensional carbon material. Unlike carbon nanotubes, GNSs consist of a monolayer graphene curled spirally on itself. TEM observations of water inside a GNS revealed a few-nanometer-thick water film left on the inner surface after recession of the meniscus. The film broke down into ripples aligned along the length which looked similar to that reported for liquids inside a tube under microgravity conditions [18], which followed the Plateau-Rayleigh (PR) instability. However, the distance between adjacent ripples was markedly different. In this Letter, we propose an idea to explain the observed results using a linear instability theory, considering the disjoining pressure between ultrathin water films and graphene layers into the theory. The PR instability was proposed to explain the breakup of a liquid column into isolated droplets or plugs [18,19,21]. It is important for applications such as film coatings of fibers and capillary tubes [22], inkjet printing, nanomaterial growth, [23,24], and cell sorting [25]. At the macroscale, surface tension is essential for the instability [18,19,21,26], whereas the van der Waals interactions could play an important role at the nanoscale [27–30].

GNSs containing water [Fig. 1(a)] were fabricated by a scoop-up method inspired by the sample preparation technique proposed by Mirsaidov *et al.* [13]. They encapsulated a droplet of water on a graphene layer with another graphene layer for TEM observations. Here, we scooped up a floating graphene-poly(methyl methacrylate) (PMMA) layer in water with a graphene-covered TEM grid. This was followed by removal of the PMMA layer by immersing the grid in acetone and water and drying it to obtain the GNSs. Water inside the GNSs was observed with a TEM (JEM-2100 Plus Electron Microscope, JEOL Ltd., Tokyo, Japan) at a 120 kV or 200 kV accelerating voltage (see Supplemental Material [31]). The GNS, as shown in Fig. 1, was cylindrical with inner diameters ranging over 64.4–71.2 nm depending on their location. The GNS contained water and gas that were respectively

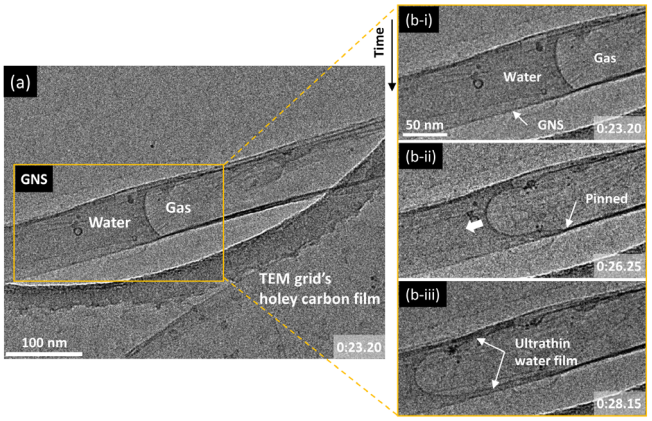

FIG. 1. TEM images of a GNS filled with water and gas. (a) Image at the start of the water-meniscus recession. (b) Sequence of close-up views during the recession of the meniscus. Water and gas are respectively represented by dark and bright areas (b-i). After the meniscus started to recede, the three-phase contact line was pinned (b-ii), leaving a thin liquid film on the inner surface of the GNS (b-iii).

distinguished by dark and bright areas, according to different densities. Electron energy loss spectroscopy (EELS) of another sample confirmed the presence of water (Fig. S1, see Supplemental Material, which includes Refs. [32,33]). Water was entrapped in the GNS, and the gas may consist of entrapped air, vapor and/or hydrogen generated by water radiolysis owing to electron-beam irradiation [34]. Water was clearly distinct from gas because of the few-nanometer-thick graphene layers. A close-up view [Fig. 1(b)] shows the meniscus of the water column receding, likely because of the electron-beam irradiation. Initially, the GNS was filled with water on the left side [Fig. 1(b–i)]. When the meniscus started to recede, the three-phase contact line stopped moving [Fig. 1(b–ii)], consequently leaving a thin liquid film on the inner surface of the GNS [Fig. 1(b–iii)]. The thickness of the liquid film was less than 8 nm. The sequence of the processes in Fig. 1(b) is shown in Movie S1.

The liquid film was unstable on the graphene surface and started to form ripples (Fig. 2 and Movie S2, following Fig. 1 and Movie S1). This behavior was analogous to the formation of liquid plugs from an annular liquid film inside 5–9 mm diameter tubes in a microgravity environment [18]. Usually, this would be analyzed with the PR instability theory. However, the GNS inner diameter and the film thickness were more than 5 orders of magnitude smaller. Unlike previous reports, the ripples finally reshaped into a thinner film likely because of the water radiolysis produced by continuous electron-beam irradiation [Fig. 2(a)].

The distances between adjacent ripples ranged over 32.2 to 64.8 nm and were greater near the meniscus [Fig. 2(b)]. The average distance between the ripples, 47.6 ± 5.4 nm, was considerably smaller than that predicted from the PR instability theory. The fastest-growing wavelength λ_0

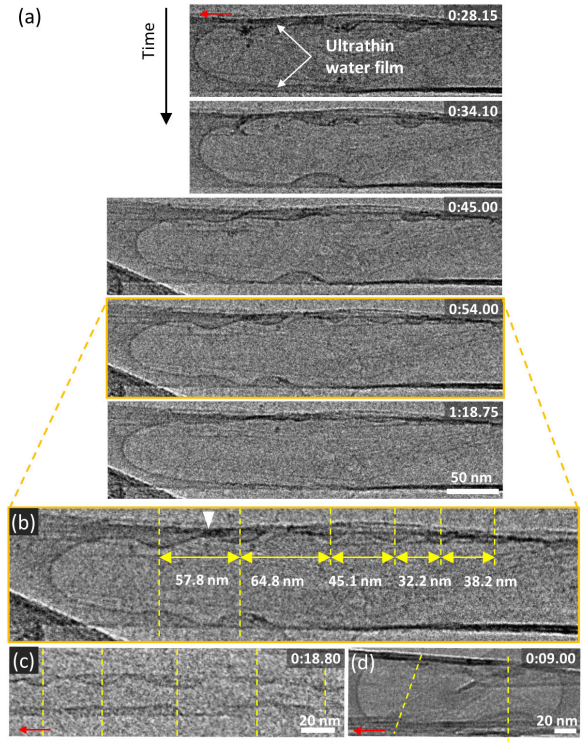

FIG. 2. Nanoscale instability of an ultrathin water film inside a GNS. (a) Time sequence of TEM images of the interfacial fluctuation. (b) Enlarged image of the separated ripples. Yellow double-headed arrows indicate distances between ripple peaks. The distances ranged over 32.2 to 64.8 nm. They were smaller than the fastest-growing wavelength, $\lambda_0 \approx 230$ nm of the disturbance on a uniform annular liquid film for the radius r_g of the gas core in the GNS, as expected with the PR instability theory. At the point shown by the white triangle in (b), the liquid film was pinned by contamination. (c), (d) Ripples observed with different GNSs. The red arrows in (a), (c), (d) indicate the direction of the meniscus recession.

of the disturbance on a uniform annular liquid film (i.e., the distance between ripples), is given by [21]

$$\lambda_0 = 2\sqrt{2}\pi r_g \tag{1}$$

where r_g is the radius of the gas core [see Fig. 3(a)]. The value of λ_0 for r_g in the GNSs was greater than ≈230 nm, which is approximately 5 times the observed value. The formation of ripples was also observed in other GNSs [Figs. 2(c) and 2(d), and Movies S3, S4]. Although the GNS diameter and the liquid-film length were different because they were uncontrollable, the mean distances between ripples, 46.9 ± 2.7 nm [Fig. 2(c)] and 87.7 ± 5.1 nm [Fig. 2(d)], were only 44% of $\lambda_0 \approx 106$ nm and 43% of $\lambda_0 \approx 206$ nm, respectively.

The presence of contaminations or defects was unavoidable in the experiments (Figs. 1 and 2). For example, contamination at the point indicated by the white triangle in Fig. 2(b) pinned the film. However, even if one ripple was

influenced by a contamination nearby, the others were not and aligned along the length. Therefore, the purpose of this work was to elucidate a potential mechanism for ripple formation by accounting for nanoscale effects in the PR instability theory.

When a liquid film has a nanometer-scale thickness, it is affected by the disjoining pressure from van der Waals interactions with the solid interface. The potential of disjoining pressure is given by $P_{\mathrm{vdW}} = -A/12\pi D^2$, where A is the Hamaker constant and D is the distance between the two interfaces [35]. To estimate this factor for a liquid film inside a GNS, we assume that the film is placed between a gas and graphene. The other side of the graphene is a vacuum environment [Fig. 3(b)]. Thus, the potential of the van der Waals interaction becomes [27,35,36]

$$P_{\mathrm{vdW}}(h) = -\frac{A_{\text{water-water}} - A_{\text{water-graphene}}}{12\pi h^2} - \frac{A_{\text{water-graphene}}}{12\pi(h + h_{\mathrm{gr}})^2} \tag{2}$$

where h and h_{gr} are the thicknesses of the water film and the graphene, respectively. The Hamaker constants are $A_{\text{water-water}} = 3.7 \times 10^{-20}$ J [35] for the interaction between water and water, $A_{\text{graphene-graphene}} = 9 \times 10^{-21}$ J [37] for the interaction between graphene and graphene, and $A_{\text{water-graphene}} = \sqrt{A_{\text{water-water}} A_{\text{graphene-graphene}}}$ for the interaction between water and graphene. We used the approximation $A_{12} \approx \sqrt{A_{11} A_{22}}$ [35] for estimating $A_{\text{water-graphene}}$ instead of using the Lifshitz theory. Although we assumed the air and the vacuum at both sides, P_{vdW} was independent of the gas component because the Hamaker constants of the air, vacuum, water vapor, and hydrogen were close to zero. We assumed a few graphene layers, thus, $h_{\mathrm{gr}} \approx 1$ nm.

Regarding the instability of a water film on graphene layers, we made the following assumptions: (1) the liquid flows as an incompressible viscous Newtonian fluid; (2) gravitational effects are ignored because all length scales are considerably smaller than the capillary length of water ($l_c = 2.7$ mm); (3) inertial and viscoelastic effects are neglected because the Reynolds number (3×10^{-9}) is many orders of magnitude smaller than 1 (see Supplemental Material) [19] and the estimated Weissenberg number of water is 0.065 [20]; and (4) there is no slippage at the solid-liquid interface. We consider a disturbance in a uniform annular liquid film with thickness e. The thickness along the x direction is $h = e + u$, where the disturbance u is given by

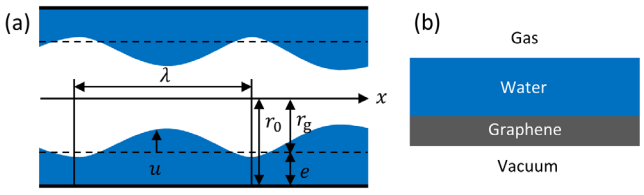

FIG. 3. Schematics of (a) physical model and coordinate system for the linear instability theory and (b) the three-interface system for calculation of the Hamaker constant to determine the disjoining pressure from van der Waals interactions.

$$u(x,t) = u_0 \exp(iqx) \exp(\omega t) \tag{3}$$

where t is time, u_0 and q are the initial amplitude and the wave number of the disturbance, respectively, and ω is the growth rate of the disturbance. The perturbation of the thickness causes a pressure modulation, which in turn induces a flow J in the film [21]:

$$J = \frac{e^3}{3\eta}\left(-\frac{dp}{dx}\right) \tag{4}$$

where η is the dynamic viscosity of the liquid. The pressure p is the sum of Laplace and disjoining pressures [21]:

$$p = \gamma\left(-\frac{\partial^2 u}{\partial x^2} - \frac{1}{r_0 - (e+u)}\right) + P''(e)u \tag{5}$$

where $P''(e) = -((A_{\text{water-water}} - A_{\text{water-graphene}})/2\pi e^4) - (A_{\text{water-graphene}}/2\pi(e + h_{\mathrm{gr}})^4)$ and r_0 is the inner radius of the GNS. From the conservation of volume, i.e., $\partial u/\partial t + \nabla \cdot J = 0$, and Eqs. (3)–(5), with an assumption $u \ll e$, we obtain

$$\omega = -\frac{e^3\gamma}{3\eta}\left[q^4 - \frac{1}{\gamma}\left(\frac{\gamma}{(r_0 - e)^2} - P''(e)\right)q^2\right]. \tag{6}$$

Figure 4(a) plots the growth rate of the disturbance as a function of wavelength $\lambda(= 2\pi/q)$ for various liquid-film thicknesses e over the range 1–8 nm, assuming $r_0 = 33.9$ nm for the case shown in Fig. 2(b). The growth rate transitions from negative to positive at the critical wavelength λ_c, given by

$$\lambda_c = 2\pi\left[\frac{1}{\gamma}\left(\frac{\gamma}{(r_0 - e)^2} - P''(e)\right)\right]^{-1/2}. \tag{7}$$

Therefore, disturbances with wavelengths $\lambda > \lambda_c$ increase with time because $\omega > 0$; whereas, those with $\lambda < \lambda_c$ are suppressed. At any film thickness, there are disturbances with positive ω, suggesting that an annular liquid film is always unstable.

The disturbance that has the maximal growth rate $\omega_{\max}$ at $\lambda_{\max}$ will grow most rapidly. The fastest-growing wavelength $\lambda_{\max}$, is given by

$$\lambda_{\max} = 2\pi\left[\frac{1}{2\gamma}\left(\frac{\gamma}{(r_0 - e)^2} - P''(e)\right)\right]^{-1/2}. \tag{8}$$

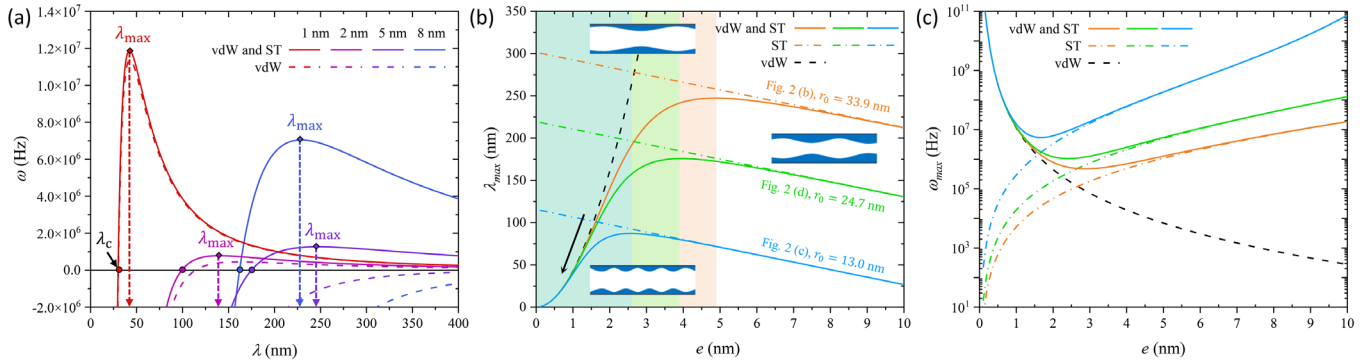

FIG. 4. (a) Dispersion relations for perturbation with the disturbance wavelength for various film thicknesses $e = 1$, 2, 5, 8 nm. (b) Effect of van der Waals interactions and surface tension on the fastest-growing wavelength vs film thickness for various GNS diameters shown in Figs. 2(b)–2(d). (c) The growth rate of the fastest growing disturbance shown in (b). The arrow in (b) indicates that λ_{max} decreases for e less than 4.9, 3.9, and 2.6 nm in each case, because of the disjoining pressure that becomes prominent at thinner films. Solid lines are the results from our theory that considered the van der Waals interactions and the surface tension. The dot-dashed lines are from the PR instability theory, and the dashed lines are the results calculated only with the effect of the van der Waals interactions.

The first term is the contribution of surface tension and the second term originates from the disjoining pressure. Figure 4(b) plots λ_{max} as a function of film thickness e for given GNS diameters that correspond to the cases in Figs. 2(b)–2(d). The value of λ_{max} increased monotonically as e decreased because of the surface tension [dot-dashed line in Fig. 4(b)]. However, it then decreased because the disjoining pressure became dominant for thinner films. The results indicated that λ_{max} was almost independent of r_0 and became smaller with decreasing e at $e < \approx 1.5$ nm, while it significantly depended on r_0 at larger e values, as in the case of the PR instability, and had a maximum value. The value of e yielding λ_{max} that matched the distance between adjacent ripples observed in the experiments (30–90 nm) was $\approx$0.9–1.5 nm. Therefore, the theory suggested a potential mechanism of instability that is caused by nanometer-thick liquid films. Figure 4(c) plots the growth rate of the disturbance for λ_{max} as a function of e. With decreasing e, the value of ω_{max} became smaller but increased suddenly at $e < \approx 1.5$ nm. The estimated 10^6–10^7-Hz-growth rate of the fastest-growing disturbance was considerably higher than the observations and those estimated by molecular dynamics simulations [30,38].

The hypothesized mechanism of forming ripples based on these results is as follows: after the meniscus recedes, a disturbance with a longer wavelength starts growing mostly due to the PR instability. Although the disturbance grows rapidly at the rate of $\approx 10^7$ Hz in the initial stage where the linear instability analysis assumed $u \ll e$, it slows down because of large deformation of the surface ($u \approx e$) and a limited volume of liquid in the thin film, forming a visible ripple ($u \gg e$). During the process of thinning the liquid film, due to efflux of water to the ripple, other disturbances with smaller wavelengths start growing at higher growth rates due to the disjoining pressure. Thickness, the dominant parameter in the instability, depends both on the thinning rate of the liquid film and the growth rate of disturbance. Therefore, the thickness could not be specified in the experiment due to not only the recession of the meniscus and consequent formation of the liquid film. This complex mechanism may be a reason why the ripple formation did not occur simultaneously but fluctuated.

Our theoretical analysis contains several assumptions that deserve further discussion. One is the assumption that the GNS has a circular cross section. If a GNS has a flat cross section instead, a liquid will be trapped at two corners because of the curvature effect. Once trapped [Fig. S3(b)], liquid with a concave interface would be stable, and would not show the surface-tension-driven instability (see Supplemental Material). Only when the film becomes much thinner, would the van der Waals interaction induce the instability. This is probably one of the reasons why the behavior shown here was not observed frequently. Our second assumption is that the graphene-water interface is no-slip. Despite the large slip at the interface is unique to the water-graphene interaction [6], the analysis using a strong slip model [40] demonstrated that the slip length influenced the growth rate of the disturbance, but did not significantly affect the fastest-growing wavelength or its dependence on liquid-film thickness (Fig. S5). The assumption of a uniform temperature was reasonable because the electron beam was parallel and uniform within the observed area, and heating of the sample was negligible [41]. Furthermore, the relationship between the fastest-growing wavelength and the liquid-film thickness was almost independent of whether the curvature was considered or not into the Hamaker constant (Fig. S4) [39].

The mechanism provided above was our hypothesized interpretation of the observed phenomena. The key factor is the van der Waals interactions that induce rapidly growing disturbances of liquid films thinner than $\approx$1.5 nm. It is likely that the phenomena were affected by many

uncontrollable factors such as deviation from a uniform circular cross section and constant diameter of the GNSs, some contamination and/or defects in the graphene, and electron beam irradiation during observation. These may have resulted in longitudinally nonuniform and fluctuated ripple formations. However, without the effect of the van der Waals interactions we cannot explain the formation of these ripples after the liquid-film formation. It should be noted that an additional calculation by changing the Hamaker constant from $A_{\text{graphene-graphene}}$ to $A_{\text{BN-BN}} = 7.64 \times 10^{-19}$ J [42] provided an interesting insight that a water film thinner than 2 nm will be stable in boron nitride nanotubes (Fig. S6). We hope to conduct future experiments with boron nitride nanotubes to test this prediction.

In summary, we have shown that a water film that is a few nanometers in thickness remains on a graphene surface during the recession of the meniscus inside a GNS. The breakup of the film occurred in GNSs with diameters over the range 26–70 nm. This behavior was similar to that in millimeter-diameter capillary tubes, resulting in the formation of ripples. The intervals between ripples in the GNSs were considerably smaller than those predicted by the PR instability theory. Therefore, we have incorporated the van der Waals interactions between the nanoscale water film and the graphene layers. This term considerably reduced the fastest-growing wavelength, particularly for liquid films less than ≈5 nm depending on the GNS inner diameter. In addition, the growth rate increased dramatically for liquid films thinner than ≈1.5 nm. The analysis indicated the instability of the liquid film due to the van der Waals interactions. We hope that these findings will be useful in tailoring liquid management inside nanofluidic systems and porous materials. Examples include liquid-water layers in electrode pores for high-density performance in polymer electrolyte fuel cells [43], and liquid-filling three-dimensional graphene and CNT-based wicks for liquid-vapor phase change heat transfer [44].

The authors would like to thank Professor Koji Takahashi at Kyushu University for his support in the use of the TEM facility and for discussion of the results. The authors also thank Dr. Pablo Sols-Fernndez from Kyushu University for his assistance in improving the graphene transfer technique, and Dr. Masaki Kudo from Kyushu University for his assistance in the EELS analysis of water at the Ultramicroscopy Research Center at Kyushu University. We also thank Sofia Di Toro Wyetzner for editing the English text of a draft of this manuscript. This work was partially supported by the Japan Society for the Promotion of Science Grants-in-Aid for Scientific Research (KAKENHI) (Grants No. JP19K23490, No. JP20K14668, and No. JP20J13061), and the Japan Science and Technology Core Research for Evolutional Science and Technology (CREST) (Grant No. JPMJCR18I1).

*Corresponding author.
ytomo@mech.kyushu-u.ac.jp

[1] L. Bocquet, Nat. Mater. **19**, 254 (2020).
[2] J. Rabinowitz, C. Cohen, and K. L. Shepard, Nano Lett. **20**, 1148 (2020).
[3] X. Liang and S. Y. Chou, Nano Lett. **8**, 1472 (2008).
[4] S. P. Surwade, S. N. Smirnov, I. V. Vlassiouk, R. R. Unocic, G. M. Veith, S. Dai, and S. M. Mahurin, Nat. Nanotechnol. **10**, 459 (2015).
[5] A. Siria, P. Poncharal, A.-L. Biance, R. Fulcrand, X. Blase, S. T. Purcell, and L. Bocquet, Nature (London) **494**, 455 (2013).
[6] E. Secchi, S. Marbach, A. Niguès, D. Stein, A. Siria, and L. Bocquet, Nature (London) **537**, 210 (2016).
[7] G. Hummer, J. C. Rasaiah, and J. P. Noworyta, Nature (London) **414**, 188 (2001).
[8] K. Koga, G. Gao, H. Tanaka, and X. C. Zeng, Nature (London) **412**, 802 (2001).
[9] K. V. Agrawal, S. Shimizu, L. W. Drahushuk, D. Kilcoyne, and M. S. Strano, Nat. Nanotechnol. **12**, 267 (2017).
[10] F. M. Ross, Science **350** (2015).
[11] N. Naguib, H. Ye, Y. Gogotsi, A. G. Yazicioglu, C. M. Megaridis, and M. Yoshimura, Nano Lett. **4**, 2237 (2004).
[12] M. P. Rossi, H. Ye, Y. Gogotsi, S. Babu, P. Ndungu, and J.-C. Bradley, Nano Lett. **4**, 989 (2004).
[13] U. Mirsaidov, V. Mokkapati, D. Bhattacharya, H. Andersen, M. Bosman, B. Özyilmaz, and P. Matsudaira, Lab Chip **13**, 2874 (2013).
[14] Q.-Y. Li, R. Matsushita, Y. Tomo, T. Ikuta, and K. Takahashi, J. Phys. Chem. Lett. **10**, 3744 (2019).
[15] Y. Tomo, A. Askounis, T. Ikuta, Y. Takata, K. Sefiane, and K. Takahashi, Nano Lett. **18**, 1869 (2018).
[16] L. M. Viculis, J. J. Mack, and R. B. Kaner, Science **299**, 1361 (2003).
[17] X. Xie, L. Ju, X. Feng, Y. Sun, R. Zhou, K. Liu, S. Fan, Q. Li, and K. Jiang, Nano Lett. **9**, 2565 (2009).
[18] H. Takamatsu, M. Fujii, H. Honda, and H. Uchiyama, Microgravity Sci. Technol. **12**, 2 (1999).
[19] S. Haefner, M. Benzaquen, O. Bäumchen, T. Salez, R. Peters, J. D. McGraw, K. Jacobs, E. Raphaël, and K. Dalnoki-Veress, Nat. Commun. **6**, 7409 (2015).
[20] T. J. O'Sullivan, S. K. Kannam, D. Chakraborty, B.-D. Todd, and J. E. Sader, Phys. Rev. Fluids **4**, 123302 (2019).
[21] P.-G. De Gennes, F. Brochard-Wyart, and D. Quéré, *Capillarity and Wetting Phenomena: Drops, Bubbles, Pearls, Waves* (Springer Science & Business Media, New York, 2013).
[22] B. Primkulov, A. Pahlavan, L. Bourouiba, J. W. Bush, and R. Juanes, J. Fluid Mech. **886** (2020).
[23] R. W. Day, M. N. Mankin, R. Gao, Y.-S. No, S.-K. Kim, D. C. Bell, H.-G. Park, and C. M. Lieber, Nat. Nanotechnol. **10**, 345 (2015).
[24] H. Suzuki, T. Kaneko, Y. Shibuta, M. Ohno, Y. Maekawa, and T. Kato, Nat. Commun. **7**, 11797 (2016).
[25] M. Chabert and J.-L. Viovy, Proc. Natl. Acad. Sci. U.S.A. **105**, 3191 (2008).
[26] S. L. Goren, J. Fluid Mech. **12**, 309 (1962).
[27] R. Seemann, S. Herminghaus, and K. Jacobs, Phys. Rev. Lett. **86**, 5534 (2001).

[28] A. A. Pahlavan, L. Cueto-Felgueroso, A. E. Hosoi, G. H. McKinley, and R. Juanes, J. Fluid Mech. **845**, 642 (2018).
[29] B. Zhao, A. A. Pahlavan, L. Cueto-Felgueroso, and R. Juanes, Phys. Rev. Lett. **120**, 084501 (2018).
[30] C. Zhao, J. E. Sprittles, and D. A. Lockerby, J. Fluid Mech. **861** (2019).
[31] See Supplemental Material at http://link.aps.org/supplemental/10.1103/PhysRevLett.128.144502 for details on sample preparations and TEM imaging, EELS analysis, estimation of Reynolds number, notes of the shape of a GNS, curvature effect, and slip length effect, and estimation for a boron nitride nanotube.
[32] T. Pylkkänen, A. Sakko, M. Hakala, K. Hämäläinen, G. Monaco, and S. Huotari, J. Phys. Chem. B **115**, 14544 (2011).
[33] L. Å Näslund, J. Lüning, Y. Ufuktepe, H. Ogasawara, Ph. Wernet, U. Bergmann, L. G. M. Pettersson, and A. Nilsson, J. Phys. Chem. B **109**, 13835 (2005).
[34] N. M. Schneider, M. M. Norton, B. J. Mendel, J. M. Grogan, F. M. Ross, and H. H. Bau, J. Phys. Chem. C **118**, 22373 (2014).
[35] J. N. Israelachvili, *Intermolecular and Surface Forces* (Academic Press, New York, 2015).
[36] B. Bera, N. Shahidzadeh, H. Mishra, L. A. Belyaeva, G. F. Schneider, and D. Bonn, Appl. Phys. Lett. **112**, 151606 (2018).
[37] R. Rajter, R. French, W. Ching, W. Carter, and Y. Chiang, J. Appl. Phys. **101**, 054303 (2007).
[38] Y. Zhang, J. E. Sprittles, and D. A. Lockerby, Phys. Rev. E **102**, 053105 (2020).
[39] D. Mattia, V. Starov, and S. Semenov, J. Colloid Interface **384**, 149 (2012).
[40] M. Rauscher, R. Blossey, A. Munch, and B. Wagner, Langmuir **24**, 12290 (2008).
[41] J. M. Grogan, N. M. Schneider, F. M. Ross, and H. H. Bau, Nano Lett. **14**, 359 (2014).
[42] T. M. Mohona, A. Gupta, A. Masud, S.-C. Chien, L.-C. Lin, P. C. Nalam, and N. Aich, Environ. Sci. Technol. **53**, 4161 (2019).
[43] U. Pasaogullari and C. Wang, J. Electrochem. Soc. **151**, A399 (2004).
[44] R. Wen, X. Ma, Y.-C. Lee, and R. Yang, Joule **2**, 2307 (2018).